Transport, Damping, and Wave-Couplings from Chaotic and Collisional Neoclassical Transport

C. Fred Driscoll, Andrey A. Kabantsev, and Daniel H. E. Dubin* and Yu. A. Tsidulko†

*Department of Physics, University of California at San Diego, La Jolla, CA USA 92093-0319
†Budker Institute of Nuclear Physics, 11 Lavrentieva prospect, Novosibirsk, 630090, Russia

Abstract. Experiments and theory characterize the novel chaotic neoclassical transport scaling as $\nu_c^0 B^{-1}$ in contrast to traditional collisional neoclassical transport scaling as $\nu_c^{1/2} B^{-1/2}$. This chaotic transport occurs when local trapping separatrices have θ-variations or temporal fluctuations. Experiments observe bulk particle transport, damping of Langmuir waves and diocotron waves, and nonlinear wave-wave couplings. These effects may be important in low-collisionality fusion plasmas.

Keywords: particle transport, wave damping
PACS: 52.25.Gj, 52.25.Dy, 52.27.Jt, 52.55.Jd

INTRODUCTION

This paper gives an overview of experimentally observed neoclassical transport and damping effects, distinguishing the novel "chaotic" effects from the standard collisional effects.

The neoclassical transport is due to global field errors which break cylindrical symmetry, combined with a separatrix creating locally trapped populations of particles. The chaotic enhancement occurs when the separatrix is "ruffled" in the drift direction, or fluctuating in time, and may be prominent in cylindrical non-neutral plasmas and in magnetic fusion devices such as stellarators.

The five effects described here include bulk particle transport [1, 2, 3, 4, 5], damping of drift [6] and Langmuir [7] waves, and modified nonlinear wave-wave couplings [8]. Experiments and theory distinguish traditional collisional effects from the novel chaotic effects, with chaotic effects dominating in regimes of low collisionality.

For strong magnetic fields ($B > 1$ kG here), effects due to locally-trapped particle populations are often dominant, and relatively simple "bounce-averaged" neoclassical theory is effective [2, 4, 6]. In this regime, *collisional* separatrix crossings give rates scaling as $\nu_c^{1/2} B^{-1/2}$, whereas chaotic separatrix crossings due to θ-ruffles or temporal fluctuations give rates scaling as $\nu_c^0 B^{-1}$, i.e. *independent* of collisionality. Experiments demonstrate that magnetic ripples as small as $\delta B/B \sim 10^{-3}$ can produce significant trapped-particle effects, and that electrostatic fluctuations with $e\delta\phi \sim T$ cause significant chaotic separatrix crossings just as effectively as do spatial ruffles or traditional collisions.

For low magnetic fields, resonances between z-kinetics and θ-drifts are apparently

dominant, making the theory more complex. Experimentally observed transport rates scale approximately as $B^{-2.7}$, roughly consistent with resonant particle transport calculations.

Theory analyses which include trapped particles and ruffled separatrix effects have now been developed from two complementary perspectives, and are in fair quantitative agreement with experiments. A dynamical bounce-mapping approach characterizes the quasi-steady-state density perturbations, including bounce-resonant effects in regimes of ultra-low collisionality. A second bounce-averaged approach [2, 4, 9] assumes random (chaotic) separatrix crossings, connects smoothly with collisional transport, and agrees with the dynamical approach outside the bounce-resonant regimes.

Experimentally, quiescent pure electron plasmas are confined close to the rotating thermal equilibrium states made possible by the azimuthal trap symmetry [10]. Controlled transport and damping effects are then induced by applying "global field errors" such as magnetic field tilt; and the transport is enhanced by trapped particles and collisional or chaotic separatrix dissipation.

In this paper, we review two effects of *applied field errors*:
1) bulk radial transport, increasing the mean-square-radius and of the plasma at rate $\nu_{\langle r^2\rangle}$; and
2) damping of $\ell_\theta > 0$, $k_z = 0$ drift (diocotron) modes at rate $\gamma_{\ell d}$.

Three similar wave damping effects are observed with *no applied field errors*, when the wave itself is the θ-dependent error field. Observed effects include
3) damping of the $\ell_\theta > 0$, $k_z(+/-)$ Trapped Particle Diocotron Mode;
4) damping of $\ell_\theta > 0$, $k_z > 0$ plasma (Langmuir) modes; and
5) modified nonlinear wave-wave couplings, when waves ruffle the separatrix.

Finally, we relate these results to toroidal stellarator geometry, where the toroidal curvature always provides a strong global field error, and particles trapped in magnetic field ripples give rise to "superbanana" neoclassical transport. We suggest that chaotic transport discussed here may dominate over the theoretically analyzed ν_c^1 and $\nu_c^{1/2}$ collisional regimes, especially in fusion-relevant plasmas where the collisionality ν_c is small.

APPARATUS

The pure electron plasma columns utilized here are confined in a cylindrical Penning-Malmberg trap [5], with magnetic field $0.4 < B < 20$ kG (Fig. 1). The electron columns have length $L_p = 49$ cm, and radial density profile $n(r)$ with central density $n_0 = 1.6\times10^7\text{cm}^{-3}$ and line density $N_L = \pi R_p^2 n_0 = 6.1\times10^7$ cm^{-1}. The equilibrium potential gives an $E\times B$ drift-rotation frequency $f_E(r)$ which decreases monotonically from $f_{E0} = 230\,\text{kHz}\cdot(B/1\,\text{kG})^{-1}$. The electrons have a near-Maxwellian velocity distribution with thermal energy $T \lesssim 1$ eV, giving axial bounce frequency $f_b \equiv \bar{v}/2L_p \lesssim 430$ kHz.

An electrostatic trapping barrier with separatrix energy ϕ_s is created at $z = 0$ by a "squeeze" wall voltage V_{sq} having adjustable strength "ruffles" with azimuthal variation m_θ. This gives interior separatrix energy $\phi_s(r,\theta) = \phi_{s0}(r) + \Delta\phi_m(r)\cos[m(\theta-\theta_m)]$. Here, we consider $m = 2$ ruffles only, created by voltages $\pm\Delta V_m$ applied to four 60° sectors,

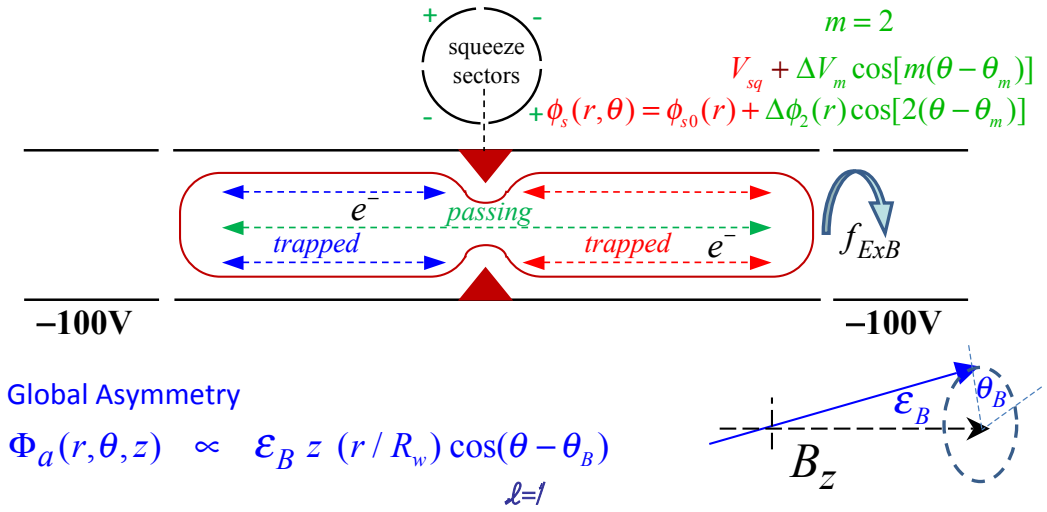

FIGURE 1. Cylindrical trap schematic, showing plasma with trapping barrier created by applied wall squeeze voltages, and with global field error from a controlled magnetic field tilt.

with $\theta_m = 0.22\pi$. At every plasma radius, low energy particles are trapped in either the left or right end, whereas higher energy untrapped particles transit the entire length.

Particles change from trapped to untrapped (and vice versa) due to collisions, due to drift-rotation across θ-ruffles $\Delta\phi_m$, or due to temporal fluctuations $\Delta\phi_t$ in the separatrix energy. The electron-electron collisionality of the present experiments is relatively low; collisions acting for a drift-rotation period spread parallel velocities at the separatrix [6, 11, 9] by an energy width $\Delta W_c \equiv (\nu_c/2\pi f_E)^{1/2}(\phi_{s0}T)^{1/2} \approx 20\,\mathrm{meV}\cdot(B/1\,\mathrm{kG})^{1/2}$. The "chaotic" processes will be important when $\Delta\phi_m \gtrsim \Delta W_c$, or when $\Delta\phi_t \gtrsim \Delta W_c$.

BOUNCE-AVERAGED NEOCLASSICAL DIFFUSION

Radial transport is driven by global "error fields" varying as $\delta\phi_\ell \sim e^{i\ell\theta}Z(z)$; here, we consider $\ell = 1$ only; and we use ℓ (rather than m) for the field error θ-variation. For our transport data, the error field is created by a small magnetic tilt with controlled magnitude $\varepsilon_B \equiv B_\perp/B_z \lesssim 10^{-3}$ and chosen tilt direction $\theta_B \equiv \tan^{-1}(B_y/B_x)$, i.e. rotated by

$$\alpha \equiv \theta_B - \theta_m \tag{1}$$

relative to the ruffle. This tilt is equivalent to applying wall voltages $V(R_w,\theta,z) = (\varepsilon_B z)(2eN_L/R_w)\cos(\theta - \theta_B)$, which causes interior Debye-shielded $\ell = 1$ error fields $\delta\phi_1(r,z)$.

When there are trapped particles, bounce-averaged neoclassical transport arises from the difference in drifts in the left and right z-averaged error fields $\overline{\delta\phi}_L$ and $\overline{\delta\phi}_R$, with step size $\Delta r^2 = [(\overline{\delta\phi}_L - \overline{\delta\phi}_R)/\frac{\partial}{\partial r}\Phi_e]^2$. (These bounce-averaged effects will be distinguished from bounce-resonance "kinetic" effects later in Fig. 4.) Collisions randomly trap or detrap a particle fraction $F_M(\phi_s)\Delta W_c$ in a rotation period, where F_M is the Maxwellian distribution of energies. Similarly, separatrix m_θ-ruffles of amplitude $\Delta\phi_m$ chaotically

trap or detrap a fraction $F_M \Delta\phi_m$, and temporal fluctuations of amplitude $\Delta\phi_t$ chaotically trap or detrap a fraction $F_M \Delta\phi_t$. One thus obtains [1, 2, 4, 9] a radial diffusion coefficient

$$D_r = f_E \, \Delta r^2 \frac{1}{4} F_M(\phi_{s0}) \{ \, \Delta W_c D_{cA} \, + \, \Delta\phi_m D_{mA} \sin^2 \ell\alpha \, + \, \Delta\phi_t D_{mA} \, \}, \tag{2}$$

with "collisional bounce-Averaged" coefficient $D_{cA} \lesssim \pi$; "m-ruffle bounce-Averaged" coefficient $D_{mA} \approx 4$; and the $\sin^2 \ell\alpha$ term represents a varying dynamical symmetry which reduces the effective step size.

BULK EXPANSION RATE $\nu_{\langle r^2 \rangle}$ (1)

Experimentally, we diagnose the bulk expansion rate

$$\nu_{\langle r^2 \rangle} \equiv \frac{d}{dt} \langle r^2 \rangle / \langle r^2 \rangle \, , \;\; \text{with} \;\; \langle r^2 \rangle \equiv \int 2\pi r \, dr \;\, n \;\, r^2 / N_L. \tag{3}$$

Fortunately, $\nu_{\langle r^2 \rangle}$ can be accurately and readily obtained from the *frequency* f_{20} of a weak diagnostic $m = 2$, $k = 0$ diocotron mode, as $\nu_{\langle r^2 \rangle} = -\frac{d}{dt} f_{2d} / f_{2d}$. This follows from $f_{2d} \propto \langle n \rangle = N_L / 2\pi \langle r^2 \rangle$ with N_L constant; and it has been verified to $\pm 2\%$ by camera images of plasma evolutions.

Figure 2 shows measured expansion rates $\nu_{\langle r^2 \rangle}$ versus magnetic tilt direction θ_B, for various applied wall ruffle strengths ΔV_m. The ruffled-induced chaotic transport shows an unambiguous $\sin^2 \alpha$ dependence, with magnitude proportional to ΔV_m, adding to the θ_B-independent collisional component. For alignments with $\alpha = 0$, the ruffle *reduces* the collisional transport slightly (solid bars), in agreement with theory showing a decrease in D_{cA} due to ruffle-induced transitions (Fig. 3). Both components scale as ε_B^2 for $\varepsilon_B \lesssim 1$ mrad, transitioning into the $\varepsilon_B^{1/2}$ (banana) regime [12] for larger tilts.

The distinctive $\sin^2 \alpha$ signature, together with control of V_{sq}, ΔV_m and ε_B, enables experimental identification of bounce-averaged effects separately from bounce-rotation resonance (i.e., kinetic) effects. Fig. 4 shows the observed magnetic field scalings (symbols, dashed lines) together with bounce-averaged theory estimates (solid lines). Here, C_{cA} and C_{mA} represent radial integrals of the bounce-averaged D_r. The C_{cK1} and C_{cK2} coefficients represent "standard" plateau-regime transport, with collisions randomizing bounce-resonant (kinetic) orbit steps driven by the tilt and ruffle error fields. The residual $\nu_{\langle r^2 \rangle}^{(\mathrm{bkg})}$ represents transport from *uncontrolled* background error fields, separatrices, and ruffles. The theory calculations are radial integrals of diffusion and associated mobility [9] from the Debye-shielded fields $\delta\phi_\ell(r)$, $\phi_{s0}(r)$ and $\Delta\phi_m(r)$.

At high B, the chaotic and collisional neoclassical coefficients C_{mA} and C_{cA} agree well with theory, scaling as B^{-1} and $B^{-1/2}$ respectively. Here the comparison is limited by temperature uncertainty, sensitivity to edge density gradients, and induced modification of $F_M(\phi_{s0})$. At low B, the collisional kinetic transport labeled C_{cK1} is observed to depend strongly on field ($\sim B^{-2.7}$), but no simple power-law is expected as bounce-rotation resonances become dominant [12]. Prior transport scaling experiments [5] have been

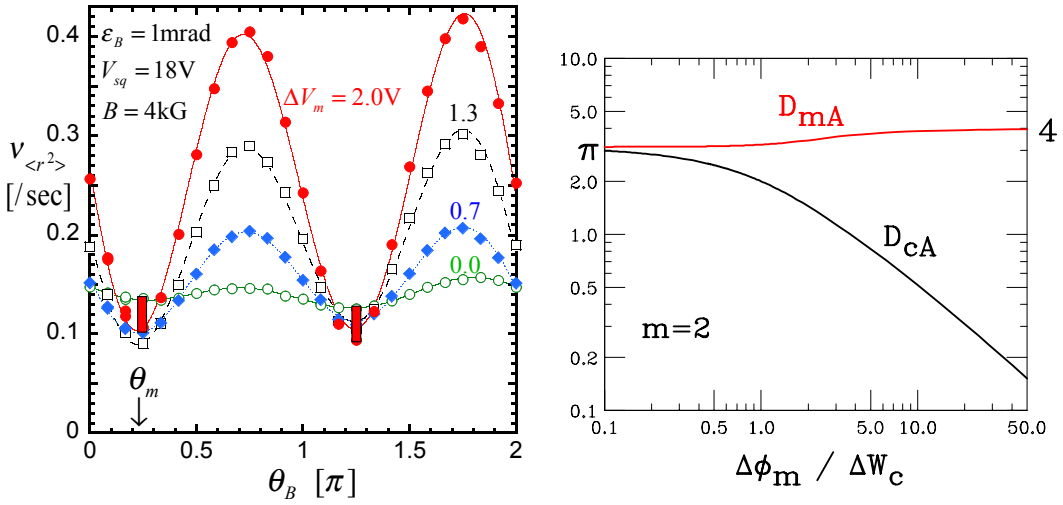

FIGURE 2. (Left) Measured bulk expansion rate $\nu_{\langle r2\rangle}$ versus magnetic tilt direction θ_B for 4 different ruffle voltages ΔV_m. Note that the ruffle-induced chaotic transport reduces the collisional transport (bars) *only* for the 2 specific alignments of $\alpha = 0, \pi$.

FIGURE 3. (Right) Calculated bounce-Averaged diffusion coefficients D_{mA} and D_{cA} from m_θ ruffles and collisions respectively, versus ruffle strength as characterized by the ratio of separatrix spreading widths $\Delta\phi_m/\Delta W_c$.

confused by the presence of uncontrolled separatrices and ruffles, and by overlapping transport regimes.

Similar chaotic transport is observed when there are *temporal* variations $\Delta\phi_t$ in the separatrix energy. Figure 5 illustrates the immediate (but reversible) increase in radial expansion rate when white noise of rms amplitude $\Delta V_t \sim 0.2\ V$ is applied to the θ-

$$\nu_{\langle r^2\rangle} = C_{cA}\,\hat{\varepsilon}_B^2 + C_{mA}\,\hat{\varepsilon}_B^2\,\Delta\hat{V}_m \sin^2(\alpha) + C_{cK1}\,\hat{\varepsilon}_B^2 + C_{cK2}\,\Delta\hat{V}_m^2 + \nu_{\langle r^2\rangle}^{(bkg)}$$

$$\Delta\hat{V}_m \equiv \Delta V_m / 1.\text{Volt}$$

$$\hat{\varepsilon}_B \equiv \varepsilon_B / 1\text{mRad}$$

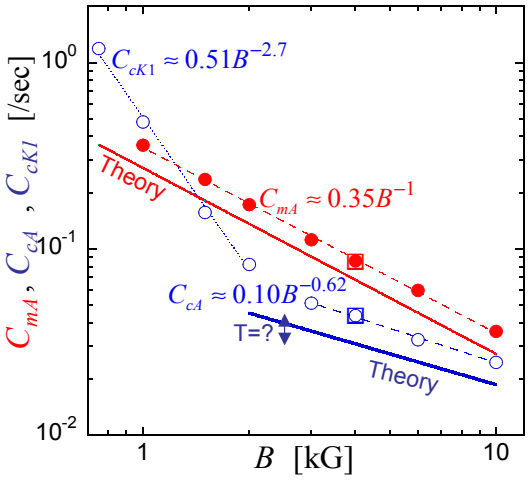

FIGURE 4. Measured Bulk expansion coefficients versus magnetic field B. Coefficients C_{mA}, C_{cA} represent ruffle-induced and collision-induced neoclassical transport in the bounce-Averaged regime; and C_{cK1} represents Kinetic effects such as bounce-resonant transport. Solid lines represent theory estimates in the bounce-Averaged regime.

symmetric squeeze ring, causing chaotic trapped-passing transitions. The $3\times$ increase in $(d/dt)\langle r^2\rangle$ observed here is consistent with a collisional separatrix layer $\Delta W_c \sim 70$ meV fluctuating by $\Delta\phi_t \sim 200$ meV. Presumably, any noise or wave-induced fluctuations which change particle kinetic energies relative to the separatrix energy would be equally effective in enhancing transport.

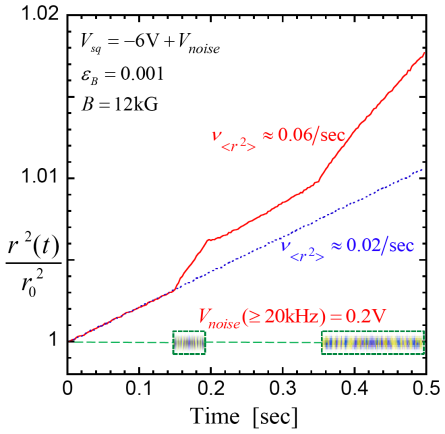

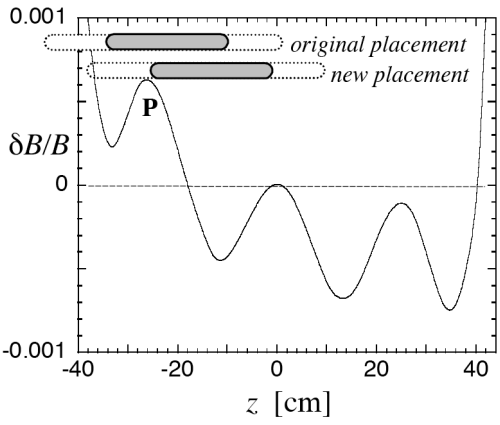

FIGURE 5. (Left) Bulk plasma expansion due to an applied tilt is enhanced $3\times$ during an applied wall "noise" voltage which causes trapping barrier fluctuations $\Delta\phi_t$.

FIGURE 6. (Right) Plot of vendor-specified magnetic field strength versus z shows a $\delta B/B \sim 10^{-3}$ peak which causes plasma expansion when positioned within the confinement region.

MAGNETIC RIPPLE TRAPPING

Trapped particles arising from weak magnetic mirroring give rise to similar enhanced transport effects. The superconducting magnet used for the present experiments has a (gratuitous) magnetic peak with $\delta_B/B \sim 10^{-3}$, interior to our original axial position for the containment electrodes, as shown in Fig. 6. By positioning this peak at the end of the containment electrodes, "background transport" was decreased [5] by a factor of $5\times$.

The 10^{-3} mirror is expected to trap about 3% of the particles, and this causes strong superbanana transport. Interestingly, adding a stronger mirror does not seem to increase the transport, possibly because the magnetic separatrix covers the entire range of $v_{\|}$ and $v_{\perp}$. Experimentally, the magnetic separatrix is substantially harder to control and vary, so our experiments have focused on electrostatic barriers.

$\ell_\theta > 0$ DIOCOTRON DAMPING $\gamma_{\ell d}$ (2)

Damping of $k_z = 0$ diocotron (drift) modes with $\ell_\theta = 1, 2$ is observed when a global field error such as tilt acts on trapped particle populations created by a central squeeze voltage. It is now clear from experiments and theory that this damping is intimately related to particle diffusion and transport, in both the chaotic and collisional regimes.

Figure 7 shows the measured $\ell = 2$ diocotron mode damping rate, γ_{2d}, versus magnetic tilt direction θ_B; also shown is the bulk expansion rate $\nu_{\langle r2\rangle}$, measured on the same plasma at the same time. The same distinctive $sin^2(\alpha)$ variation is observed in both

measurements, and scalings with magnetic field strength reveal the same collisional and chaotic scalings of $B^{-1/2}$ and B^{-1} respectively.

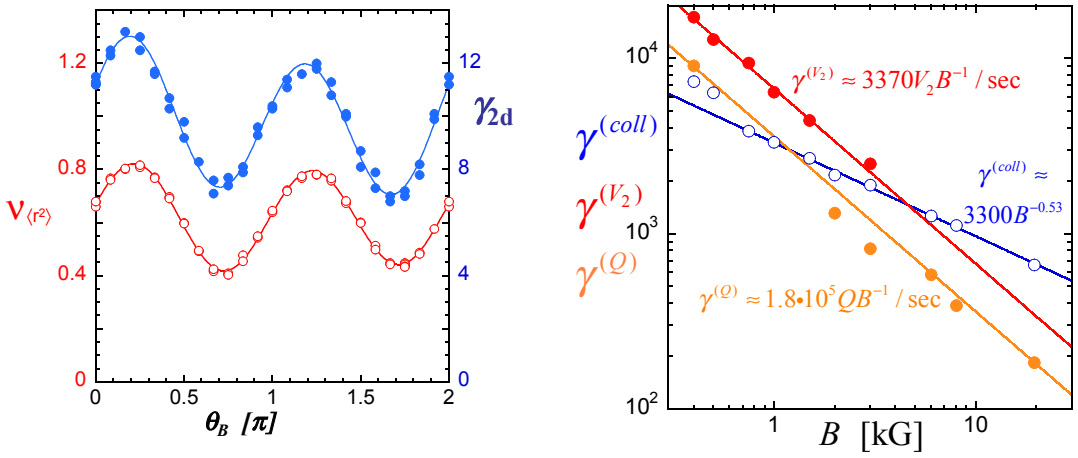

FIGURE 7. (Left) Measured damping of the $m_\theta = 2$ diocotron mode (γ_{2d}) due to separatrix and magnetic tilt shows exactly the same $\sin^2(\alpha)$ dependence as does bulk plasma expansion $\nu_{\langle r2\rangle}$.

FIGURE 8. (Right) Measured TPDM damping rates γ_{1a} versus B due to a separatrix with *no* applied magnetic tilt, showing the separate contributions from collisions (coll), from a static applied $m_\theta = 2$ ruffle (V2), and from a separately launched $m_\theta = 2$ diocotron mode (Q).

$\ell_\theta > 0$, $k_z(\pm)$ TRAPPED PARTICLE DIOCOTRON MODE DAMPING (3)

We now discuss three wave damping effects where the wave itself constitutes the global field error, in the sense of driving the neoclassical separatrix dissipation. This requires that the wave have $\ell_\theta \neq 0$ and $k_z \neq 0$, so that it breaks cylindrical symmetry and acts differently on the separate trapped populations. Here, there is no applied magnetic tilt ε_B, and various tests establish that the damping is independent of any remaining trap asymmetries.

In one sense, these damping experiments merely demonstrate the theoretical adage that "damping is the flip side of transport." One important distinction is that with wave-induced damping, the dissipation continues until the wave is abated; wheres with asymmetry-induced transport, the dissipation continues until the plasma is abated.

Historically, the appearance and damping of the Trapped Particle Diocotron Mode was the first effect noticed when a squeeze was applied to the middle of cylindrical pure electron plasma [5, 6]. The mode is anti-symmetric in z (and was initially called the "Asymmetry Mode"); it can have any ℓ_θ, but we focus on $\ell_\theta = 1$.

In extremis, the TPDM is two separate diocotron modes, 180 degrees out of phase with each other, each supported by the separately drifting trapped particles, somewhat shielded by the passing particles, and damped by trapped/passing separatrix transitions. The TPDM frequency decreases continuously from f_E to the "standard" diocotron

frequency f_{1d} as the squeeze increases towards "cut-off"; and the TPDM damping rate correspondingly decreases.

Initial theory work analyzed the TPDM damping in terms of traditional collisional separatrix dissipation [11]. This gave a $B^{-1/2}$ scaling in correspondence with strong-field experiments, but did not explain the B^{-1} scaling observed at lower magnetic fields.

A key theory insight introduced by Tsidulko in 2008 was that even weak $m_\theta = 2$ (or higher) ruffles on a nominally theta-symmetric separatrix can be as effective as weak collisions in producing damping and transport.

Figure 8 shows the measured $\ell_\theta = 1$ TPDM damping rates $\gamma = \gamma_{1a}$ versus magnetic field. Here, we are able to experimentally distinguish 3 effects causing separatrix transactions: collisions, giving $\gamma^{(\mathrm{coll})}$; an applied *static* $m_\theta = 2$ ruffle on the separatrix, giving $\gamma^{(V_2)}$; and a *wave-induced* separatrix ruffle from a separately launched "standard" $m_\theta = 2$ diocotron mode giving $\gamma^{(Q)}$. Here, the collisional $B^{-1/2}$ and chaotic B^{-1} scalings are clearly observed over 2 decades in magnetic field.

DAMPING OF $\ell_\theta > 0$, $k_z > 0$ PLASMA MODES (4)

Damping from separatrix dissipation can readily dominate the theoretically beloved Landau damping, and is effective even in the "BGK" wave-trapped-particle states. Moreover, even weak magnetic ripples cause moderately strong damping.

Figure 9 shows the measured damping rates for an $\ell_\theta = 1$, $k_z = 1\ \pi/L_p$ Langmuir mode at $f_{11} \sim 1.2$ MHz which as been excited to large amplitude, with $\delta n/n \sim 0.3$. Here, a linear wave would be *overdamped* (with $\gamma/f_{11} \sim 2$); but the wave persists in a BGK state for a thousand wave cycles.

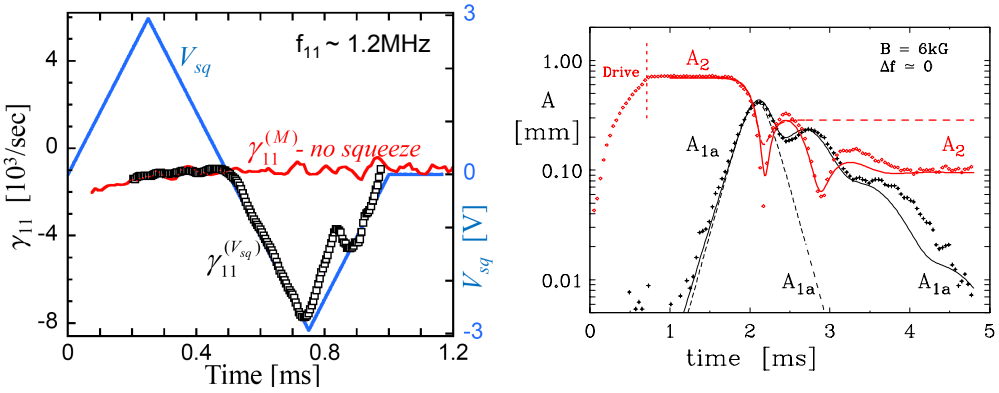

FIGURE 9. (Left) Instantaneous damping rate $\gamma_{\|}^{(t)}$ of an $\ell_\theta = 1$, $k_z = 1\ \pi/L_p$ Langmuir mode is unaffected by an applied positive "anti-squeeze" voltage (blue triangular ramp); but is directly proportional to a negative θ-symmetric squeeze voltage.

FIGURE 10. (Right) Measured amplitudes versus time of a driven $\ell_\theta = 2$ diocotron mode (A_2), which decays into an $\ell_\theta = 1$ TPDM. Dashed lines are coupling theory without separatrix effects; dotted curves are improved prediction from a partial correction K.

We find that the measured "background" damping $\gamma_{11}^{(M)} \sim 10^3/\mathrm{sec}$ is due to the $\delta_B/B \sim 10^{-3}$ magnetic ripple; and that this damping is enhanced by $8\times$ when a squeeze voltage

is applied to a 360 degree cylinder. The triangular ramp of V_{sq} shows that a positive voltage has no effect, whereas a negative squeeze increases the damping proportional to the number of squeeze-trapped particles. This squeeze-enhanced damping $\gamma_{11}^{V_{sq}}$ is presumably due to collisions, and the chaotic effects of a ruffled separatrix have not yet been investigated.

RESONANT WAVE-WAVE COUPLINGS WITH SEPARATRIX DISSIPATION (5)

Separatrix dissipation, manifested either as damping or as phase shifts, can significantly alter the evolution of nonlinear wave-wave couplings.

For example, the standard $\ell_\theta = 2$ diocotron mode exhibits a decay instability into the $\ell_\theta = 1$ TPDM, if the TPDM frequency f_{1a} is adjusted to be resonant, as $f_{1a} = f_{2d}/2$. Here, the coupling is fundamentally due to the inherent nonlinearity of the convective term in the fluid or Vlasov equations, which gives a simple nonlinear coupling coefficient V. Further, one would reasonably expect that separatrix-induced TPDM damping γ_{1a} could significantly affect the time evolution of the decay instability.

Figure 10 shows the time evolution of mode amplitudes A_2 and A_{1a} when A_2 is driven to large amplitude and f_{1a} is tuned for resonance [8]. The TPDM is observed to grow from noise, then saturate and oscillate at an amplitude similar to the depleted A_2. The dashed line shows the evolution predicted from coupling coefficient V and damping γ_{1a} alone; clearly other effects are important.

Initial theory work (before chaotic transport was understood) suggested adding a nonlinear dissipative coupling term $\mathcal{K}$; and this significantly improved the prediction of late-time behavior (solid curves). It now appears that wave-induced separatrix ruffling and chaotic dissipation must be included in order to fully model the decay instability and late-time evolution, because dissipation and phase shifts are not symmetric between the two waves. This analysis is being prepared for publication.

TOROIDAL SUPERBANANA TRANSPORT

Collisional neoclassical transport theory has been extensively developed in the context of magnetic fusion energy in toroidal geometries [12, 13, 14], but few experimental tests have challenged the various theory assumptions. Prior theory [Refs. 14–16 and references therein] has considered the effect of asymmetric separatrices; however, the effect of non-zero phase angle α has not to our knowledge been previously analyzed. Moreover, some prior work treats the abrupt changes in the parallel adiabatic invariant due to separatrix crossings; but our model of differing drift dynamics of trapped and untrapped particles is quite distinct from parallel adiabatic invariant effects.

Overall, neoclassical transport has a similar structure in toroidal systems as in our cylindrical plasmas. First, toroidal curvature provides the unavoidable "global field error" which causes particles to drift off flux surfaces; this is analogous to our magnetic tilt. Second, separate populations of locally trapped and untrapped particles are created by magnetic field ripples; this is our squeeze or magnetic ripple. Third, the ripple-induced

separatrix between trapped and untrapped particles generally varies with poloidal angle around the flux surface; this is our controlled separatrix ruffle.

As shown in Fig. 11, prior collisional neoclassical transport theory predicts "super-banana" transport scaling as ν_c^1 and $\nu_c^{1/2}$ in the regimes of low collisionality of interest to MFE, and as ν_c^{-1} for large collisionality [14]. The predicted ν_c^1 regime represents the suppressed collisional transport analogous to Figs. 2 and 3 for the specific case of $\alpha = 0$. That is, ruffle-induced separatrix crossings do indeed reduce the collision-induced crossings (Fig. 3); but the $\alpha = 0$ assumption of dynamically reversible drifts is only rarely justified.

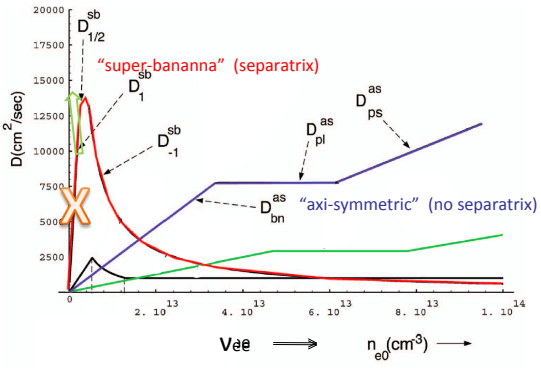

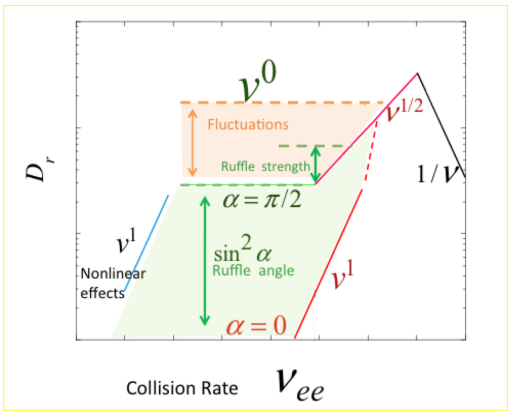

FIGURE 11. (Left) Collisional neoclassical diffusion coefficients for axisymmetric and superbanana toroidal configurations. (Re-drawn from Ref. 14) Low collisionality regimes of ν^1 and $\nu^{1/2}$ may be superceded by chaotic transport effects.

FIGURE 12. (Right) Low collisionality chaotic transport due to m_θ ruffles or due to temporal fluctuations may increase transport well above collisional predictions in ν^1 and $\nu^{1/2}$ regimes.

Similarly, the "collisional" theory assumption is that only micro-fluctuations are dynamically important in high-temperature regimes, thereby ignoring temporal fluctuations in separatrix energies due to fluctuations in plasma potential.

In contrast, our experiments and theory suggest that chaotic neoclassical transport due to ruffles or fluctuations scaling as ν_c^0 may well be dominant in regimes of low collisionality (Fig. 12). Thus, considerable work may be required to bring theory into correspondence with low-collisionality, separatrix-ruffled, fluctuating fusion plasmas.

ACKNOWLEDGMENTS

This work was supported by National Science Foundation Grant No. PHY0903877 and Department of Energy Grant DE-SC0002451.

REFERENCES

1. A. A. Kabantsev, D. H. E. Dubin, C. F. Driscoll and Yu. A. Tsidulko, Phys. Rev. Lett. **105**, 205001 (2010).

2. D. H. E. Dubin, C. F. Driscoll, and Yu. A. Tsidulko, Phys. Rev. Lett. **105**, 185003 (2010).
3. A. A. Kabantsev and C. F. Driscoll, Problems of Atomic Sci. and Tech. **6**, 26 (2010).
4. D. H. E. Dubin, A. A. Kabantsev and C. F. Driscoll, Phys. Plasmas **19**, 056102 (2012).
5. A. A. Kabantsev, C. .F. Driscoll, T. J. Hilsabeck, T. M. O'Neil, and J. H. Yu, Phys. Rev. Lett. **87**, 225002 (2001).
6. T. J. Hilsabeck, A. A. Kabantsev, C. F. Driscoll, and T. M. O'Neil, Phys. Rev. Lett. **90**, 245002 (2003).
7. A. A. Kabantsev and C. F. Driscoll, Phys. Rev. Lett. **97**, 095001 (2006).
8. A. A. Kabantsev, T. M. O'Neil, Y. A. Tsidulko and C. F. Driscoll, Phys. Rev. Lett. **101**, 065002 (2008).
9. D. H. E. Dubin and Yu. A. Tsidulko, Phys. Plasmas **18**, 062114 (2011).
10. D. H. E. Dubin and T. M. O'Neil, Rev. Mod. Phys. **71**, 87 (1999).
11. M. N. Rosenbluth, D. W. Ross, and D. P. Kostamorov, Nucl. Fusion **12**, 3 (1972).
12. D. L. Eggleston and T. M. O'Neil, Phys. Plasmas **6**, 2699 (1999).
13. P. Helander and D. J. Sigmar, *Collisional Transport in Magnetized Plasmas*, Cambridge: Cambridge Univ. Press ((2002).
14. H. Mynick, Phys. Plasmas **13**, 058102 (2006).
15. H. Mynick, Phys. Fluids **26**, 2609 (1983).
16. C. D. Beidler, Ya. I. Kolesnichenko, V. S. Marchenko, I. N. Sidorenko, and H. Wobig, Phys. Plasmas **8**, 2731 (2001).